*Protein Science* (1998), 7:132–141. Cambridge University Press. Printed in the USA.


# NMR studies of internal dynamics of serine proteinase protein inhibitors: Binding region mobilities of intact and reactive-site hydrolyzed *Cucurbita maxima* trypsin inhibitor (CMTI)-III of the squash family and comparison with those of counterparts of CMTI-V of the potato I family

JIANHUA LIU,[1] YUXI GONG,[1] OM PRAKASH,[1] LISA WEN,[2] INSUK LEE,[2]
JENQ-KUEN HUANG,[2] AND RAMASWAMY KRISHNAMOORTHI[1]

[1]Department of Biochemistry, Kansas State University, Manhattan, Kansas 66506
[2]Department of Chemistry, Western Illinois University, Macomb, Illinois 61455

(RECEIVED May 19, 1997; ACCEPTED July 5, 1997)

**Abstract**

Serine proteinase protein inhibitors follow the standard mechanism of inhibition (Laskowski M Jr, Kato I, 1980, *Annu Rev Biochem 49*:593–626), whereby an enzyme-catalyzed equilibrium between intact ($I$) and reactive-site hydrolyzed inhibitor ($I^*$) is reached. The hydrolysis constant, $K_{hyd}$, is defined as $[I^*]/[I]$. Here, we explore the role of internal dynamics in the resynthesis of the scissile bond by comparing the internal mobility data of intact and cleaved inhibitors belonging to two different families. The inhibitors studied are recombinant *Cucurbita maxima* trypsin inhibitor III (rCMTI-III; $M_r$ 3 kDa) of the squash family and rCMTI-V ($M_r \sim 7$ kDa) of the potato I family. These two inhibitors have different binding loop–scaffold interactions and different $K_{hyd}$ values—2.4 (CMTI-III) and 9 (CMTI-V)—at 25 °C. The reactive-site peptide bond ($P_1$-$P_1'$) is that between $Arg^5$ and $Ile^6$ in CMTI-III, and that between $Lys^{44}$ and $Asp^{45}$ in CMTI-V. The order parameters ($S^2$) of backbone NHs of uniformly $^{15}N$-labeled rCMTI-III and rCMTI-III* were determined from measurements of $^{15}N$ spin–lattice and spin–spin relaxation rates, and $\{^1H\}$-$^{15}N$ steady-state heteronuclear Overhauser effects, using the model-free formalism, and compared with the data reported previously for rCMTI-V and rCMTI-V*. The backbones of rCMTI-III ($\langle S^2 \rangle = 0.71$) and rCMTI-III* ($\langle S^2 \rangle = 0.63$) are more flexible than those of rCMTI-V ($\langle S^2 \rangle = 0.83$) and rCMTI-V* ($\langle S^2 \rangle = 0.85$). The binding loop residues, $P_4$-$P_1$, in the two proteins show the following average order parameters: 0.57 (rCMTI-III) and 0.44 (rCMTI-III*); 0.70 (rCMTI-V) and 0.40 (rCMTI-V*). The $P_1'$-$P_4'$ residues, on the other hand, are associated with $\langle S^2 \rangle$ values of 0.56 (rCMTI-III) and 0.47 (rCMTI-III*); and 0.73 (rCMTI-V) and 0.83 (rCMTI-V*). The newly formed C-terminal ($P_n$ residues) gains a smaller magnitude of flexibility in rCMTI-III* due to the $Cys^3$–$Cys^{20}$ crosslink. In contrast, the newly formed N-terminal ($P_n'$ residues) becomes more flexible only in rCMTI-III*, most likely due to lack of an interaction between the $P_1'$ residue and the scaffold in rCMTI-III. Thus, diminished flexibility gain of the $P_n$ residues and, surprisingly, *increased* flexibility of the $P_n'$ residues seem to facilitate the resynthesis of the $P_1$-$P_1'$ bond, leading to a lower $K_{hyd}$ value.

**Keywords:** binding loop; dynamics; NMR; potato I family; protein inhibitor; serine proteinase; squash family

Serine protease protein inhibitors function according to the standard "lock and key" mechanism (Laskowski & Kato, 1980; Bode & Huber, 1992): when a protein inhibitor ($I$) interacts with its cognate serine protease ($E$), its reactive-site peptide bond ($P_1$-$P_1'$; Schechter & Berger, 1967) is hydrolyzed to form the clipped inhibitor ($I^*$), albeit at a much slower rate compared to that of a substrate. The cleaved form of the inhibitor, as in the case of *Cucurbita maxima* trypsin inhibitors, generally has the two polypeptide fragments connected by a disulfide bridge, and also inhibits the enzyme. Thus, in $I^*$, two binding loop fragments result, one fragment ($P_n$ residues) forming a new C terminal and the other ($P_n'$ residues) forming a new N terminal. These two fragments, which

Reprint requests to: Ramaswamy Krishnamoorthi, Department of Biochemistry, Kansas State University, Manhattan, Kansas 66506; e-mail: krish@ksu.edu.

*Abbreviations:* CMTI, *Cucurbita maxima* trypsin inhibitor; CMTI-X, *Cucurbita maxima* trypsin inhibitor X; CMTI-X*, reactive-site hydrolyzed CMTI-X; rCMTI-X, recombinant CMTI-X; rCMTI-X*, reactive-site hydrolyzed rCMTI-X; GST, glutathione-S-transferase; CPMG, Carr–Purcell–Meiboom–Gill; RMS, root mean square.

move apart from each other, however, come together at the active site of the serine protease and resynthesize the peptide bond. That involves the nucleophilic attack of the N-terminal on the carbonyl carbon of the acyl intermediate formed between the $P_1$ residue of the inhibitor and the catalytic Ser of the enzyme (Fersht, 1985). Thus, an equilibrium between intact and modified forms of a serine protease inhibitor is established, which is written as follows:

$$E + I \rightleftharpoons C \rightleftharpoons E + I^*. \quad (1)$$

In that process, the same enzyme:inhibitor complex intermediate, $C$, is formed, when the enzyme binds to $I$ or $I^*$. The equilibrium constant of hydrolysis is defined as:

$$K_{hyd} = [I^*]/[I]. \quad (2)$$

$K_{hyd}$ is thus a measure of the standard free energy change between the modified and intact forms of a given inhibitor. It is also equal to the ratio of the dissociation constants ($K^*/K_d$) of the enzyme: inhibitor complexes formed by the enzyme with $I^*$ and $I$, respectively:

$$K_d = [E][I]/[C]; K_d^* = [E][I^*]/[C]. \quad (3)$$

In certain cases, the clipped form of the inhibitor is not as effective as the intact form ($K_{hyd} > 1$).

Laskowski and coworkers have reported $K_{hyd}$ values for 42 avian ovomucoid third domains ($M_r \sim 6$ kDa; Ardelt & Laskowski, 1991), which are elastase inhibitors of the Kazal family (Laskowski & Kato, 1980). The $K_{hyd}$ values range from 0.4 to ~35 ($\Delta G^\circ_{hyd}$ ranges from −2.1 to +0.9 kcal/mol at 25 °C). Changes in $\Delta G^\circ_{hyd}$ values have been rationalized (Ardelt & Laskowski, 1991) in terms of changes in residue–residue interactions, utilizing the X-ray crystal structures determined for intact and nicked inhibitors (Weber et al., 1981; Papamokos et al., 1982; Bode et al., 1985; Musil et al., 1991), and the complex formed between turkey ovomucoid third domain and *Streptomyces griseus* protease B (Fujinaga et al., 1982). The NMR solution structures of intact and clipped forms of turkey ovomucoid third domain (Krezel et al., 1994; Walkenhorst et al., 1994) suggest that the nascent terminals move apart from each other and that there is no salt bridge formed between them. Recently, it has been demonstrated (Qasim et al., 1997) that the free energy changes of association of enzyme–inhibitor complexes formed between six different proteases and the same $P_1$ mutants of two serine protease inhibitors belonging to two different families—eglin *c* of the potato I family and turkey ovomucoid domain of the Kazal family—are similar. That study suggests that binding loop properties are largely independent of the protein scaffold, because the two inhibitor families have different scaffolding designs.

A limitation in the use of X-ray crystal structures for the rationalization of $K_{hyd}$ values of a large number of protein inhibitors is the neglect of internal dynamics. Internal motions of a protein on different time scales, extending from picosecond to second, have been suggested to play an important role in its functions, such as ligand binding, enzyme catalysis, antibody recognition, etc. (Karplus & McCammon, 1983; Karplus, 1986). Dynamics also influences protein stability and folding (Richards, 1992). Unfolded proteins are typically more flexible than native structures.

We have performed extensive NMR studies on CMTI-V ($M_r \sim 7$ kDa; Fig. 1A), a potato I family member, and characterized differences in the structural, functional, thermodynamic, and dynamic properties of both intact and modified inhibitor (Krishnamoorthi et al., 1990; Cai et al., 1995a, 1995b, 1996; Wen et al., 1995; Liu et al., 1996a, 1996b). The $K_{hyd}$ of CMTI-V is ~9 at 25 °C, pH 6.8, and, as expected, the modified form shows a reduction in its inhibitory activity toward trypsin and factor XIIa, a serine proteinase involved in blood coagulation (Cai et al., 1995b). Structural and dynamical changes are mainly confined to the reactive-site region (Cai et al., 1995b; Liu et al., 1996b). However, in the clipped form of the recombinant inhibitor, rCMTI-V*, the $P_n$ residues of the newly formed C terminal acquire considerable internal mobility, whereas the $P_n'$ residues of the newly formed N terminal remain as rigid as in the intact form (Liu et al., 1996b). Both these fragments remain attached to the protein scaffold by the hydrogen bonding side chains of $Arg^{52}$ and $Arg^{50}$, respectively, as in the intact form (Liu et al., 1996b). The decreased binding affinity of CMTI-V* appears to be consistent with the increased flexibility of the $P_n$ fragment. This has led us to raise the following question: if there are two serine proteinase protein inhibitors belonging to two different families and possessing different $K_{hyd}$ values for the trypsin-catalyzed equilibrium, can we gain an insight into the role of internal dynamics of the binding loop fragments in the resynthesis of the $P_1$-$P_1'$ bond from a comparative study?

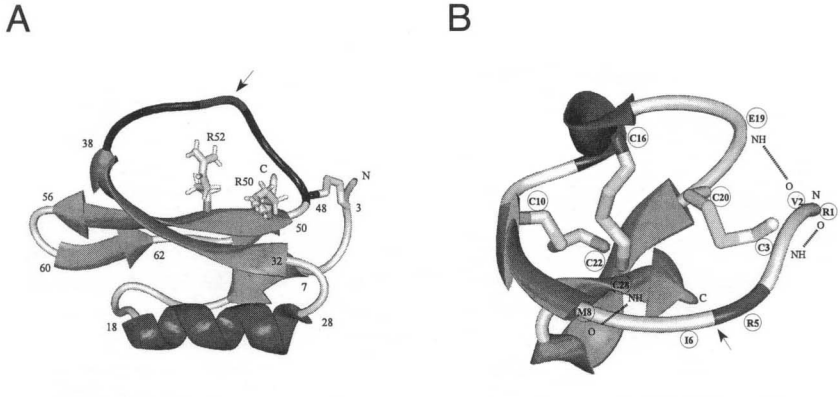


**Fig. 1.** Ribbon representations of the three-dimensional structures of (**A**) CMTI-V (Liu et al., 1996a) and (**B**) CMTI-I (Bode et al., 1989), showing the binding loop anchors to the protein scaffold. See text for details. Arrow identifies the reactive-site peptide bond ($P_1$-$P_1'$) in each case.

What we have asked here involves *not a direct correlation* between internal dynamics and $K_d$ or $K_d^*$ for a pair of inhibitors, *but a comparison between relative values of the ratio,* $K_d^*/K_d$ (i.e., $K_{hyd}$), and the binding loop dynamics of intact and clipped forms of the two inhibitors. Because each family of serine proteinase protein inhibitors is characterized by a particular pattern of scaffolding and amino acid sequence of the binding loop region (Laskowski & Kato, 1980), a comparative study of *changes* in the internal mobilities of binding loop residues between intact and clipped states for the two inhibitors is anticipated to provide clues into the role of internal dynamics in the mechanism of inhibition. Specifically, such a comparison may shed light on the role of internal dynamics of the binding loop fragments in the resynthesis of the scissile bond.

CMTI-III (~3 kDa), a member of the squash family (Wieczorek et al., 1985; for a review, see Otlewski & Krowarsch, 1996), provides an excellent system for comparison with the much-studied potato I family member, CMTI-V. Both the crystal (Bode et al., 1989) and the solution structure (Holak et al., 1989a, 1989b, 1991) have been determined for CMTI-I, the natural E9K mutant of CMTI-III (Fig. 1B). Natural and chemical variants of the squash inhibitor have been demonstrated to inhibit physiologically important serine proteinases, such as factor XIIa (Hojima et al., 1982; Krishnamoorthi et al., 1990; Wynn & Laskowski, 1990; Hayashi et al., 1994), cathepsin G (McWherter et al., 1989), and plasmin (Otlewski et al., 1990). Solution NMR studies of CMTI-III* and CMTI-I*, as well as the thermodynamics of the trypsin-catalyzed equilibrium, CMTI-III $\rightleftharpoons$ CMTI-III*, have been reported (Krishnamoorthi et al., 1992a, 1992b). The $K_{hyd}$ of CMTI-III is ~2.4 at 25 °C, pH 4.7. The $K_{hyd}$ of CMTI-I, which is similar to that of CMTI-III, has been found to undergo no significant change between pH 4 and 7.5 (Otlewski & Zbyryt, 1994).

The scaffolding patterns differ between the potato I and squash families of inhibitors: in CMTI-V (Fig. 1A; Cai et al., 1995a; Liu et al., 1996a), the reactive-site loop (residues 40–49) is held in position by two hydrogen bonds—the $Arg^{50}$ side chain anchoring the $P_n'$ segment and the $Arg^{52}$ side chain holding in position the $P_n$ region. The $Cys^3$–$Cys^{48}$ crosslink provides additional support for the $P_n'$ region. On the other hand, in CMTI-III (or CMTI-I; Fig. 1B; Bode et al., 1989), the $P_n$ region of its binding loop is attached to the scaffold by a disulfide bond ($Cys^3$–$Cys^{20}$) and a hydrogen bond ($Val^2 \cdots Glu^{19}$); similarly, the $P_n'$ portion is supported by a hydrogen bond ($Met^8 \cdots Cys^{28}$) and a disulfide bridge ($Cys^{10}$–$Cys^{22}$). Thus, the differences in the binding loop interactions with the scaffold for the two inhibitors, together with the different $K_{hyd}$ values determined at 25 °C [2.4 for CMTI-III (Krishnamoorthi et al., 1992b) and ~9 for CMTI-V (Cai et al., 1995b)], have motivated the present comparative study of internal mobilities of the binding loop residues in intact and clipped forms of both inhibitors.

## Results

### *Assignments of $^1H$-$^{15}N$ chemical shift correlation spectra of rCMTI-III and rCMTI-III**

Assignments of $^{15}N$-$^1H$ cross peaks in the HSQC maps of rCMTI-III and rCMTI-III* were made by comparing the spectra with the previously assigned spectra of intact and clipped forms of the natural protein (Krishnamoorthi et al., 1992c) and confirmed by the $^{15}N$-edited 2D HSQC-TOCSY (Oschkinat et al., 1994) experiment (results not shown) in which the complete spin systems of the individual amino acid residues were correlated with the $^1H$-$^{15}N$ cross peaks. The recombinant protein has two extra N-terminal residues, $Gly^{-2}$ and $Ser^{-1}$. However, $^1H$-$^{15}N$ cross peaks of these residues were not observed in the HSQC map, most likely due to rapid exchange of the NHs with water, whose magnetization was saturated during the experiment. The $^1H$-$^{15}N$ cross peak assignments of rCMTI-III and rCMTI-III* are given in the Electronic Appendix (Figs. S-1 and S-2, respectively). The two extra N-terminal residues do not affect the overall structure of the inhibitor molecule, as confirmed qualitatively by the $^{15}N$-edited HMQC-NOESY (Oschkinat et al., 1994) experiment (results not shown). Therefore, we use the structures of intact and modified forms of the natural protein (CMTI-I; Bode et al., 1989; Holak et al., 1989a; Krishnamoorthi et al., 1992a, 1992b) for the recombinant versions as well. It was observed previously that the extra N-terminal Gly residue did not affect the structures of rCMTI-V (Liu et al., 1996a) and rCMTI-V* (Liu et al., 1996b). The entire molecule of rCMTI-III* appears to have undergone tertiary structural changes, as evidenced by $^1H$, $^{15}N$, and $^{13}C$ chemical-shift changes of its backbone and side-chain atoms (Krishnamoorthi et al., 1992a, 1992b, 1992c; Nemmers, 1992; J. Liu & R. Krishnamoorthi, unpubl. results); however, it retains the secondary structural features of the intact inhibitor (Fig. 1B)—a $3_{10}$-helix (residues 13–16) and a triple-stranded antiparallel $\beta$-sheet (residues 8–10, 27–29, and 21–25).

### *$^{15}N$ relaxation data and order parameters*

Figure 2 presents the $^{15}N$ longitudinal and transverse relaxation data, $R_1$ and $R_2$, respectively, and NOEs (Tables S-1 and S-2 in the Electronic Appendix) obtained for all the expected backbone NHs, except that of $Ser^{-1}$. For most residues, the $R_1$ values are higher in rCMTI-III than in rCMTI-III* (Fig. 2A). This is reflected in the trimmed average $R_1$ values of 2.13 ± 0.07 and 2.02 ± 0.02 $s^{-1}$ for the intact and hydrolyzed inhibitor, respectively. This trend is also noticed in the $R_2$ values (Fig. 2B). Significant differences are noted between the two forms of the inhibitor for the $R_2$ values of the binding loop residues, which form the N-terminal.

Values of 1.37 ± 0.04 and 1.42 ± 0.02 were used for the $R_2/R_1$ ratios of rCMTI-III and rCMTI-III*, respectively, to obtain their respective overall correlation times, $\tau_m$, of 1.9 ± 0.1 and 2.1 ± 0.1 ns.

The NOEs measured for residues 1–8 (Fig. 2C) show significant differences between the two forms of the inhibitor. The NOE values for $Arg^1$ and $Val^2$ are negative in both rCMTI-III and rCMTI-III*; $Cys^3$, $Arg^5$, $Leu^7$, and $Met^8$ show positive NOEs in rCMTI-III, but negative values in rCMTI-III*. Decreased or negative NOE values indicate increases in internal mobility (Peng & Wagner, 1994).

Relaxation rate constants were not determined for the two arginine side chain $N_\epsilon Hs$, because the experimental data resulted in poor $R_1$ and/or $R_2$ fitting curves; however, the relatively *large negative* NOEs observed for $Arg^1$ and $Arg^5$ indicate that both their side chains are freely mobile.

The Lipari and Szabo parameters, determined under the assumption of an overall isotropic molecular tumbling, are given in Tables S-3 and S-4 of the Electronic Appendix and displayed in Figure 3. The $S^2$ values calculated for rCMTI-III and rCMTI-III* (Fig. 3A; Tables S-3 and S-4 in the Electronic Appendix) indicate that most of the backbone is moderately constrained; however, the first three N-terminal residues, $Gly^{-2}$, $Ser^{-1}$, and $Arg^1$, and the binding loop residues 3–8, are quite flexible. Generally, rCMTI-III*

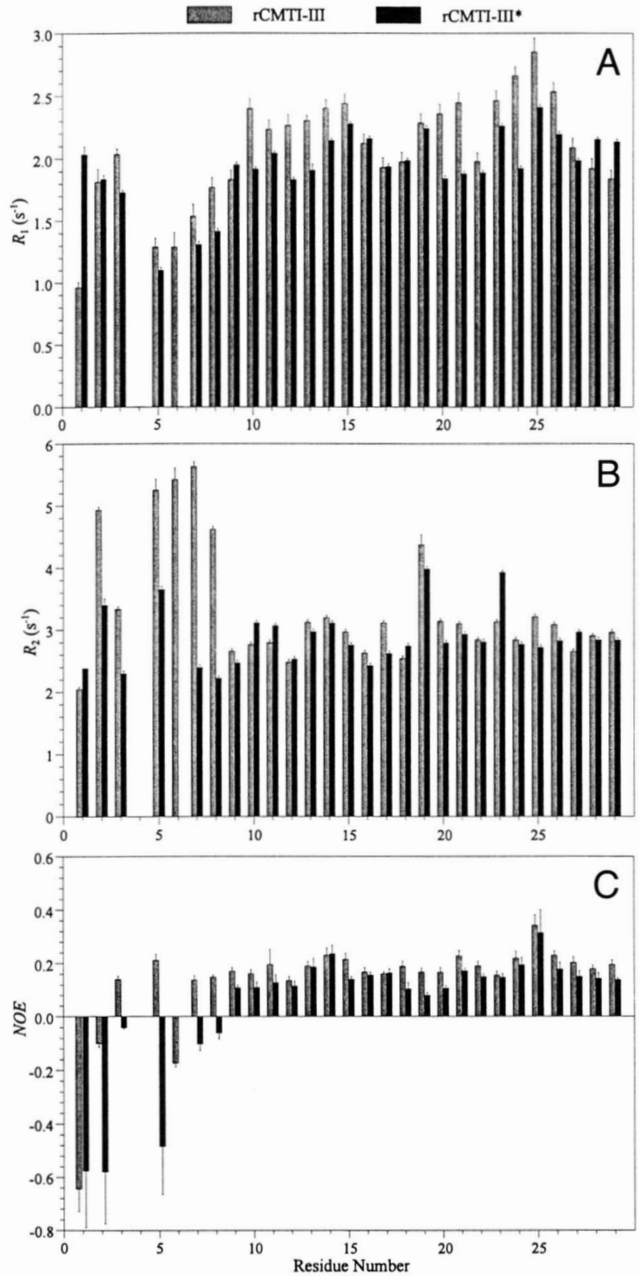


**Fig. 2.** Plot of the measured $^{15}N$ relaxation parameters as a function of amino acid residue number for rCMTI-III and rCMTI-III* at 30 °C, pH 4.7. **A:** Spin–lattice relaxation rate constants ($R_1$). **B:** Spin–spin relaxation rate constants ($R_2$). **C:** $\{^1H\}$-$^{15}N$ steady-state NOE measurements. Error bars represent standard deviations calculated from the fits to Equations 4–6 in the text. Data were not obtained for the N-terminal $Gly^{-2}$, $Ser^{-1}$, and $Pro^4$ residues; in the case of rCMTI-III*, data were not obtained for $Ile^6$.

shows lower order parameters than does rCMTI-III. The binding loop residues experience a notable increase in flexibility in the cleaved inhibitor. The effective correlation times, $\tau_e$, of most residues are within 100 ps (Fig. 3B). Conformational exchange terms are included for eight residues of rCMTI-III and seven residues of rCMTI-III* (Fig. 3C), the maximum value used being 3.7 Hz. Most of the exchange terms are associated with the binding loop residues.

## Discussion

### *Internal mobilities of rCMTI-III and rCMTI-III**

The internal correlation time, $\tau_e$, and the exchange term, $R_{ex}$, are used to account for fast (nanosecond) and slow (second) internal molecular motions, respectively, in the calculation of the model-free parameters. However, interpretation of $\tau_e$ is not attempted because of its dependence on frequency and amplitude of motion and hence, on a physical model. Similarly, the $R_{ex}$ values are not

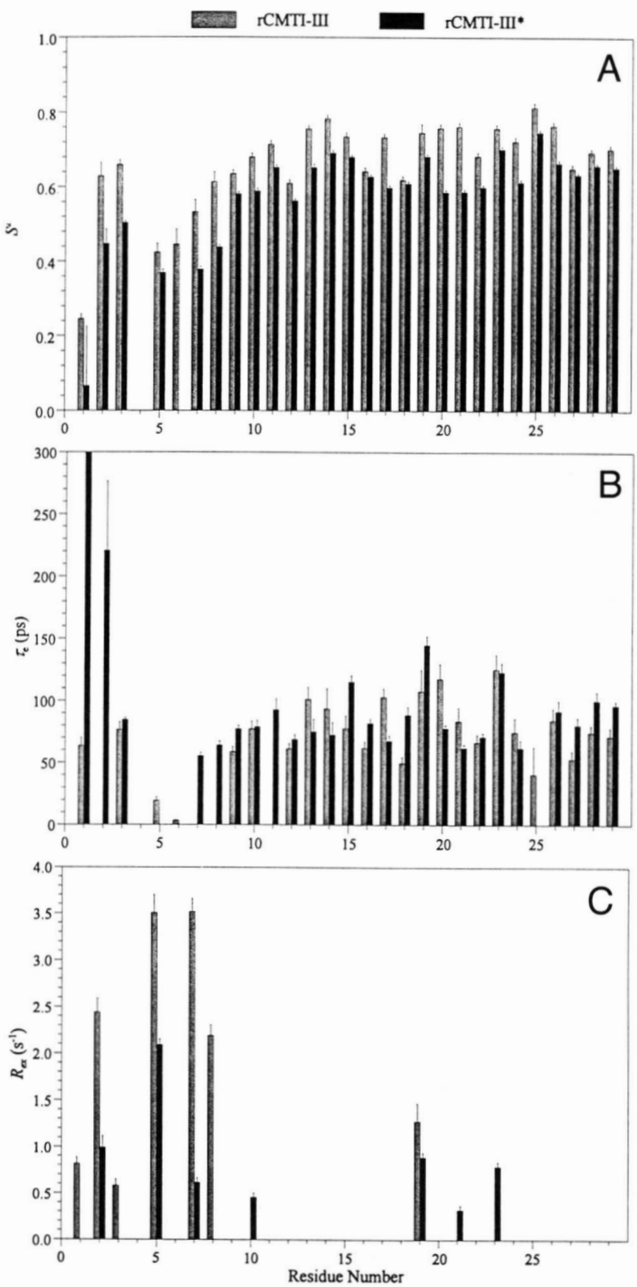


**Fig. 3.** Plot of the model-free parameters as a function of amino acid residue number for rCMTI-III and rCMTI-III*. **A:** Generalized order parameters ($S^2$). **B:** Effective internal correlation time ($\tau_e$). **C:** Chemical exchange term ($R_{ex}$). Data were not obtained for the N-terminal $Gly^{-2}$, $Ser^{-1}$, and $Pro^4$ residues; in the case of rCMTI-III*, data were not obtained for $Ile^6$.

interpreted quantitatively here, because they may simply be correction terms to experimental data to achieve a better overall fitting. However, a large $R_{ex}$ term may, in general, indicate the existence of a chemical and/or conformational exchange process. The generalized order parameter, $S^2$, is a quantitative measure of molecular flexibility or internal mobility; departure from unity for any $^{15}$N-H vector indicates the presence of internal motion that is faster than the overall molecular tumbling motion. Thus, $S^2$ values of different $^{15}$NHs in different molecules provide a measure of relative internal mobilities.

In an earlier natural abundance $^{15}$N NMR study of CMTI-III and CMTI-III* (Krishnamoorthi et al., 1992c), on the basis of a comparison of chemical shifts, we obtained additional evidence for the occurrence of tertiary structural changes throughout the molecule upon hydrolysis of the scissile bond (Krishnamoorthi et al., 1992a, 1992b). Recent analyses of order parameters in peptides and proteins using a simple model of internally restricted correlation rotations suggest that peptide NH order parameters are sensitive to structural perturbations (Daragan & Mayo, 1996). This seems to be reflected by the observed changes in order parameters (Fig. 3A). For most of the residues, the modified inhibitor shows decreased $S^2$ values. The average order parameters ($\langle S^2 \rangle$) of rCMTI-III and rCMTI-III* are 0.71 ± 0.06 and 0.63 ± 0.06, respectively, thus indicating moderately ordered backbones.

Except for the $\beta$-strand involving the C-terminal residues 27–29, all the other secondary structural elements—a $3_{10}$-helix and two $\beta$-strands—experience significant decreases in their $\langle S^2 \rangle$ values upon hydrolysis of the $P_1$-$P_1'$ bond (Table 1). The disulfide bonds of the inhibitor contribute to the backbone rigidity. Thus, peptide NHs belonging to the six Cys residues at positions 3, 10, 16, 20, 22, and 28, and some adjoining residues show increased rigidity compared to the rest of the molecule (Fig. 3A). Decrease in protein hydration has been correlated with decrease in internal flexibility in the case of bacteriorhodopsin (Fitter et al., 1996). That appears to be consistent with the increased internal mobility—especially of the binding loop fragments—of rCMTI-III*, whose reverse-phase HPLC elution behavior indicates that it is more hydrophilic (and thus more hydrated) than is rCMTI-III (Cai et al., 1996).

### *N-terminal and binding loop region (residues 1–10)*

This region shows the biggest changes in flexibility when the reactive site is hydrolyzed, as expected (Fig. 3A). The order parameters of all the binding loop residues decrease upon hydrolysis of the Arg$^5$–Ile$^6$ peptide bond, consistent with the decreased enzyme-binding affinity of the modified inhibitor. The relatively very low $S^2$ values determined for Arg$^1$ in both rCMTI-III and rCMTI-III* indicate almost completely unrestricted motion for this residue. Although lower order parameters are measured for Val$^2$ and Cys$^3$, *the magnitude of decrease in each case is no larger than observed anywhere else in the molecule—for example, residues 7, 8, 20, and 21.* This is attributable to the presence of a hydrogen bond between Val$^2$ and Glu$^{19}$ and the Cys$^3$–Cys$^{20}$ crosslink. Leu$^7$ and Met$^8$ also show decreased order parameters in the nicked inhibitor, although the latter is involved in a $\beta$-sheet. rCMTI-III shows significant $R_{ex}$ values (>1 Hz) for residues Val$^2$, Arg$^5$, Ile$^6$, Leu$^7$, and Met$^8$ (Fig. 3C; Table S-3 in the Electronic Appendix), suggesting conformational averaging motions on a time scale of seconds for these residues. In the case of rCMTI-III*, Arg$^5$ is associated with a significant $R_{ex}$ value (2 Hz).

**Table 1.** *Mean order parameters ($\langle S^2 \rangle$) of secondary structural elements in rCMTI-III and rCMTI-III**

| Secondary structure | Sequence | Number of residues | $\langle S^2 \rangle$ rCMTI-III | $\langle S^2 \rangle$ rCMTI-III* |
|---|---|---|---|---|
| $3_{10}$-Helix | 13–16 | 4 | 0.73 ± 0.02 | 0.66 ± 0.02 |
| $\beta$-Strand 1 | 8–10 | 3 | 0.64 ± 0.03 | 0.54 ± 0.02 |
| $\beta$-Strand 2 | 27–29 | 3 | 0.68 ± 0.02 | 0.65 ± 0.02 |
| $\beta$-Strand 3 | 21–25 | 5 | 0.75 ± 0.02 | 0.65 ± 0.02 |

### *Internal mobility and protein function*

Internal mobility plays an important role in protein function, as illustrated by the following few examples. In the case of a zinc finger DNA-binding domain, which has 25 amino acid residues, residues in the zinc-binding region are found to exhibit greater internal mobility compared to the rest of the molecule (Palmer et al., 1991). $^{13}$C relaxation data of staphylococcal nuclease (Nicholson et al., 1992) show that, upon ligand binding, leucine residues in the ligand-binding site lose considerable internal mobility. The side-chain dynamics of the C-terminal SH2 domain of phosphoinositol-specific phospholipase C-$\gamma$1 (Kay et al., 1996) demonstrates that residues coming into contact with the C-terminal residues of the phosphorylated tyrosine (pTyr) containing peptide are highly mobile both in free and bound state, whereas residues in the pTyr binding site are significantly restrained; that points out the dichotomous correlation between dynamics and binding specificity, on the one hand, and between dynamics and binding, on the other. Very recently, the hinge-bending motion in T4 lysozyme has been shown to be important in the opening of the active-site cleft (Mchaourab et al., 1997).

The effect of conformational flexibility on receptor–ligand binding free energy has been computed (Rosenfeld et al., 1995); for example, flexibility is credited with 30–50% of free energy change in the case of class I major histocompatibility complex receptor–peptide complexes (Vajda et al., 1994). Recent theoretical studies on globular proteins (Bhaskaran et al., 1996) indicate an inverse correlation between fluctuations and internal packing of amino acid residues, and suggest that such a correlation may be useful in identifying functionally important residues in proteins. Good correlations have been found between order parameters of amino acid residues of lysozyme and their surface accessibilities (Buck et al., 1995).

In the case of serine proteinase protein inhibitors, any correlation between binding loop flexibility and binding affinity is yet to be explored for the intact form. Dynamical studies of rCMTI-V and rCMTI-V* (Liu et al., 1996a, 1996b) have shown that the newly formed C terminal ($P_n$ segment) in rCMTI-V* becomes more flexible, whereas the newly formed N terminal ($P_n'$ fragment) remains as rigid as in the intact form. The reduced binding affinity of CMTI-V* relative to that of CMTI-V ($K_{hyd} = K_d^*/K_d \approx 9$) may be attributed to the increased flexibility of the binding loop fragment, because the other regions of the inhibitor do not undergo any significant structural or dynamical changes. Therefore, we ask whether we can obtain clues from the determination of internal dynamics of rCMTI-III and rCMTI-III* as to the increased prospects of resynthesis of the scissile bond, a necessary condition for the lower value of $K_{hyd}$ of CMTI-III (2.4), relative to that of CMTI-V (9). It is also

of interest to attribute any observed changes in internal dynamics to specific structural aspects of the binding loop anchors.

### *Comparison with rCMTI-V and rCMTI-V**

The $\langle S^2 \rangle$ values determined for the structured regions of rCMTI-V (Liu et al., 1996a) and rCMTI-V* (Liu et al., 1996b) are 0.83 and 0.85, respectively. In contrast, both rCMTI-III and rCMTI-III* show less constrained backbones with $\langle S^2 \rangle$ values of 0.71 and 0.63, respectively. Reactive-site hydrolysis significantly affects the backbone dynamics of structured regions of rCMTI-III (Table 1), but not rCMTI-V. Furthermore, residues in the $\alpha$-helix and $\beta$-sheet regions of rCMTI-V and rCMTI-V* show higher average order parameter than other residues. This is, however, not observed in rCMTI-III and rCMTI-III*. $\tau_e$ values compare well among rCMTI-III, rCMTI-III*, rCMTI-V, and rCMTI-V*, with most of the values below 120 ps. The $R_{ex}$ values observed in rCMTI-V and rCMTI-V* are less significant than those obtained for rCMTI-III.

Comparisons of the binding loop regions between rCMTI-III and rCMTI-V, and between rCMTI-III* and rCMTI-V*, are shown in Figure 4. For the intact inhibitors, the binding loop residues (except $P_3$ and $P_5'$), especially those in the $P_n'$ region, are more flexible in rCMTI-III than in rCMTI-V (Fig. 4A; Table 2). The $P_3$ residue in rCMTI-III is Cys that is crosslinked to $Cys^{20}$. In rCMTI-V, the first half of the binding loop is supported by a hydrogen bond between the side chains of $Arg^{52}$ and, most likely, $Thr^{43}$ (Liu et al., 1996b). The differences in $S^2$ values of the $P_n'$ residues of the binding loop regions in rCMTI-III and rCMTI-V probably arise from the stronger anchoring effect in rCMTI-V due to a hydrogen bond between the side chain of $Arg^{50}$ and the main-chain oxygen atom of $Asp^{45}$ (Fig. 1A; Liu et al., 1996a). In rCMTI-III, the corresponding anchor is provided by a hydrogen bond between $Met^8$ and $Cys^{28}$ (Fig. 1B; Bode et al., 1989).

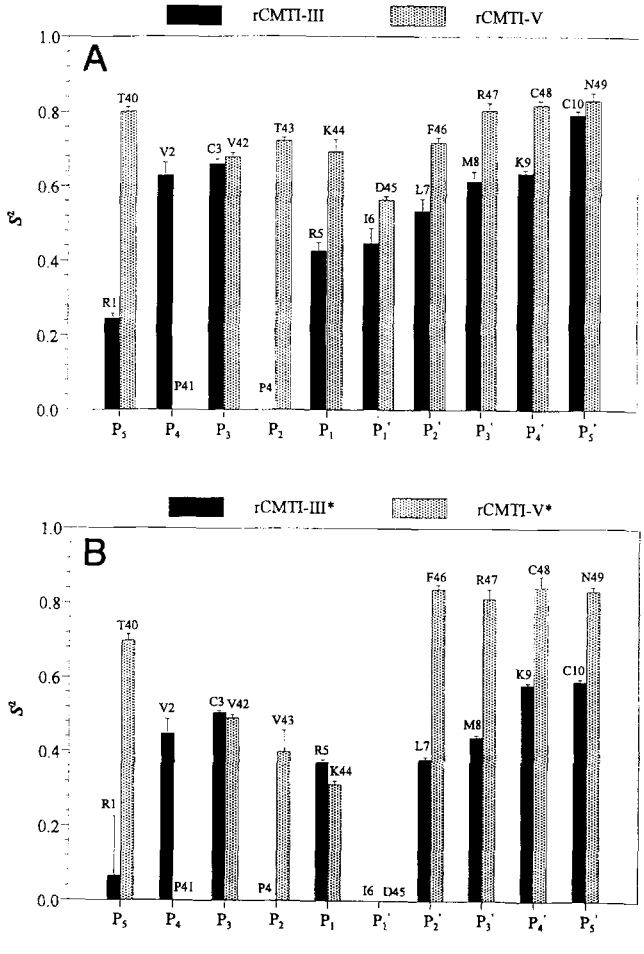


**Fig. 4.** Comparison of order parameters of binding loop residues in (**A**) rCMTI-III and rCMTI-V; and (**B**) rCMTI-III* and rCMTI-V*. Data for rCMTI-V and rCMTI-V* are taken from Liu et al. (1996a) and Liu et al. (1996b), respectively. Data were not obtained for Pro and free $P_1'$ residues in both proteins.

Disulfides have been demonstrated to play both stabilizing and destabilizing roles in different proteins (Betz, 1993). *Removal* of the disulfide bridge, $Cys^{71}$–$Cys^{101}$, near the reactive site in *Streptomyces* subtilisin inhibitor by replacement of the Cys residues with Ser residues results in the double mutant initially showing inhibitory activity similar to the wild-type protein; however, enzyme inhibition is found to be relieved with increase in time of incubation, because the hydrolyzed form is a poor inhibitor, most likely due to greater flexibility of the binding loop fragments in the mutant (Kojima et al., 1993). Removal of disulfide bridges in *Erythrina* trypsin/tissue plasminogen activator (tPA) inhibitor results in decreased thermal stability (Lehle et al., 1996). A study of four variants of staphylococcal nuclease, each of which contains an engineered disulfide bond, indicates that the presence of a disulfide has effects not only on the *folded* state, but also on the *unfolded* state, depending upon the location of the disulfide bridge (Hinck et al., 1996). Interestingly, an engineered disulfide bridge in a ferricytochrome *c* variant (connecting positions 20 and 102) makes the molecule *less* stable than the wild-type protein, whereas *local* stability, as indicated by amide H/D exchange data, near the crosslink increases (Betz et al., 1996). CMTI-III* is thermodynamically more stable than CMTI-III, i.e., $\Delta H^\circ$ is negative (Krishnamoorthi et al., 1992b). However, whether it is due partly to one or more of the three disulfides present in the molecule has not been determined. The dynamic data, on the other hand, provide evidence that the $Cys^3$–$Cys^{20}$ disulfide bond contributes to the rigidity of the $P_n$ segment of the binding loop in rCMTI-III and rCMTI-III*. This results in a smaller magnitude of increase in internal mobility that accompanies the hydrolysis reaction (Table 2).

For the modified forms of the inhibitors (Fig. 4B), interesting similarities and dissimilarities are noted: $S^2$ values of residues $P_3$-$P_1$, constituting the first half of the binding loop, are highly similar (Table 2). But, order parameter decreases observed for the residues $P_3$-$P_1$ are *smaller* for rCMTI-III* than those observed for the corresponding residues in rCMTI-V*. This is attributable to the $Cys^3$–$Cys^{20}$ disulfide bridge in rCMTI-III*. Strikingly lower $S^2$ values are observed for the $P_n'$ segment of the binding loop in rCMTI-III* than in rCMTI-V*. In rCMTI-V*, the order parameter of $Phe^{46}$ ($P_2'$ residue) increases, suggesting a strengthened hydrogen bond between $Arg^{50}$ and $Asp^{45}$ ($P_1'$ residue). The newly formed N-terminal is significantly less ordered in rCMTI-III*, because there is no anchoring interaction between the $P_1'$ residue ($Ile^6$) and the protein scaffold.

### *Internal dynamics and mechanism of inhibition*

Mechanistically, resynthesis of the reactive-site peptide bond ($P_1$-$P_1'$) involves the nucleophilic attack of the amino terminus of the $P_1'$ residue on the carbonyl carbon of the acyl intermediate formed between the $P_1$ residue and the catalytic Ser of trypsin (Fersht, 1985).

**Table 2.** *Comparison of order parameters ($S^2$) of backbone NHs of binding loop residues in intact and reactive-site hydrolyzed rCMTI-III and rCMTI-V*

| Residue[a] (rCMTI-III/rCMTI-V) | rCMTI-III | rCMTI-III* | rCMTI-V[b] | rCMTI-V*[c] |
|---|---|---|---|---|
| $P_5$ (R1/T40) | 0.25 ± 0.01 | 0.07 ± 0.16 | 0.80 ± 0.01 | 0.70 ± 0.02 |
| $P_4$ (V2/P41) | 0.63 ± 0.04 | 0.45 ± 0.04 | —[d] | —[d] |
| $P_3$ (C3/V42) | 0.66 ± 0.01 | 0.51 ± 0.01 | 0.68 ± 0.01 | 0.49 ± 0.01 |
| $P_2$ (P4/T43) | —[d] | —[d] | 0.72 ± 0.01 | 0.40 ± 0.06 |
| $P_1$ (R5/K44) | 0.43 ± 0.02 | 0.37 ± 0.01 | 0.69 ± 0.03 | 0.31 ± 0.01 |
| $P_1'$ (I6/D45) | 0.45 ± 0.04 | nd[e] | 0.56 ± 0.01 | nd[e] |
| $P_2'$ (L7/F46) | 0.53 ± 0.03 | 0.38 ± 0.01 | 0.72 ± 0.01 | 0.84 ± 0.01 |
| $P_3'$ (M8/R47) | 0.61 ± 0.03 | 0.44 ± 0.01 | 0.80 ± 0.02 | 0.81 ± 0.03 |
| $P_4'$ (K9/C48) | 0.64 ± 0.01 | 0.58 ± 0.01 | 0.82 ± 0.01 | 0.84 ± 0.03 |
| $P_5'$ (C10/N49) | 0.68 ± 0.01 | 0.59 ± 0.01 | 0.83 ± 0.02 | 0.83 ± 0.01 |

[a]According to the nomenclature of Schecter and Berger (1967). The $P_1$-$P_1'$ bond is the reactive-site peptide bond.
[b]Data taken from Liu et al. (1996a).
[c]Data taken from Liu et al. (1996b).
[d]Pro, which does not possess an NH group, occurs at this position.
[e]Not determinable because the $P_1'$ residue becomes the newly formed, second N-terminus.

From the work described, we identify two factors associated with rCMTI-III*: (1) *reduction in flexibility gain* of the $P_n$ segment due to the $Cys^3$–$Cys^{20}$ disulfide bridge; and (2) *increase in flexibility* of the $P_n'$ segment upon cleavage of the scissile bond. The resynthesis reaction is facilitated in CMTI-III ($K_{hyd}$ = 2.4, as opposed to 9 for CMTI-V). The second factor is a surprising one, because it has been thought generally that rigidity of the $P_n'$ segment would enable it to successfully compete against water molecules by virtue of increased "local" concentration of the $P_1'$ residue in the vicinity of the acyl intermediate. Structural, functional, and dynamical studies of mutants of rCMTI-V in which a disulfide bond is engineered between the $P_n$ region of the binding loop and the protein scaffold should provide further support for the first factor identified. Alternatively, the $Cys^{10}$–$Cys^{22}$ crosslink in rCMTI-III may be eliminated by the double mutation, C10S+C22S, in order to increase the flexibility of the $P_n'$ segment. Such experiments are in progress.

## Conclusions

Internal dynamics of binding loops in serine proteinase protein inhibitors belonging to two families (squash and potato I) show characteristic differences reflecting structural variations in binding loop–protein scaffold interactions. Thus, a disulfide crosslink between the $P_n$ region and the scaffold decreases the flexibility gain of the newly formed C terminal in the cleaved inhibitor. Absence of any interaction between the $P_1'$ residue and the scaffold results in increased flexibility of the newly formed N terminal. The different hydrolysis equilibrium constants measured for the representative members may, in part, be attributed to such dynamical differences. Resynthesis of the $P_1$-$P_1'$ bond seems to be better favored by a more ordered $P_1$ residue and a more flexible $P_1'$ residue.

## Materials and methods

### *$^{15}N$-labeled recombinant CMTI-III*

*Escherichia coli* strains JM109 and BL21 were used as hosts. The glutathione S-transferase (GST) fusion vector pGEX-2T (Pharmacia Biotech) was used for the expression of CMTI-III as a fusion protein with GST. The CMTI-III gene was custom-synthesized (Genosys) in the form of two overlapping oligonucleotides—CMTI-IIIF (forward) and CMTI-IIIR (reverse). The sequence of CMTI-IIIF (52-mer) was: 5′-CGC GTA TGT CCA CGC ATC TTG ATG AAA TGC AAG AAA GAT TCC GAT TGC CTG G-3′. The sequence of CMTI-IIIR (54-mer) was: 5′-CTA ACC ACA ATA GCC ATG TTC CAA GCA CAC GCA TTC TGC CAG GCA ATC GGA ATC-3′. Two-hundred nanograms of each synthetic oligonucleotide was mixed, annealed, and primer extended with the Klenow fragment (Sambrook et al., 1989). The resultant products and 100-bp DNA ladder were analyzed on a 3% agarose gel. The band at about 105 bp was excised, purified, and amplified by PCR (Perkin Elmer Cetus), using two flanking primers, CMTI-IIIF 5′ primer and CMTI-IIIR 3′ primer. The PCR product was subjected to electrophoresis on a 3% agarose gel, and the band at 105 bp was excised and isolated. The PCR-amplified gene was double-digested with *Bam*H I and *Eco*R I (both from New England Biolabs), ligated with the pGEX-2T vector, using T4 DNA ligase (New England Biolabs), and transformed into JM109 or BL21 competent cells. The recombinant DNA-containing colonies were screened by the PCR, using the CMTI-III 5′ and 3′ primer pair. The sequence of the clone was confirmed by sequencing both DNA strands with Sequenase (United States Biochemicals).

The CMTI-III gene was expressed in *E. coli* JM109 or BL21. Cells were grown in Luria-Bertani broth containing ampicillin. The recombinant protein, separated by SDS-PAGE (Laemmli, 1970) and visualized by Coomassie Brilliant Blue, was found to be expressed within 2 h and the level remained the same after overnight incubation.

For the production of uniformly $^{15}N$-labeled CMTI-III fusion protein, the *E. coli* cells were grown in a medium containing $^{15}NH_4Cl$ as the sole nitrogen source. The $^{15}N$-labeled recombinant CMTI-III was cleaved off GST by digestion with thrombin and purified by reverse-phase HPLC. The recombinant protein (yield = 3–5 mg/L of cell culture), rCMTI-III, was found to inhibit trypsin by the assay method described previously (Wen et al., 1993). The nucleic acid and amino acid sequences of rCMTI-III are as follows:

```
GGATCCCGCGTATGTCCACGCATCTTGATGAAATGCAAGAAAGATTCGATTGCCTGGCA 60
G  S  R  V  C  P  R  I  L  M  K  C  K  K  D  S  D  C  L  A   20
GAATGCGTGTGCTTGGAACATGGCTATTGTGGTTAGGAATTC 102
E  C  V  C  L  E  H  G  Y  C  G<           31
```

Thus, rCMTI-III contains two extra N-terminal amino acid residues, $Gly^{-2}$ and $Ser^{-1}$.

### *$^{15}$N-labeled recombinant CMTI-III**

rCMTI-III was reacted with trypsin (5 mol%) to produce rCMTI-III*, which was separated and purified by RP-HPLC, as described previously (Krishnamoorthi et al., 1990).

### *NMR spectroscopy*

A typical NMR sample was prepared by dissolving about 1–2 mg of the protein in 0.2 mL of 90% $H_2O$/10% $D_2O$ (v/v), which contained 50 mM KCl. The pH of the NMR sample was adjusted to 4.74 at 30 °C with 0.1 M $KO^2H$ or 0.2 M $^2HCl$, using an Ingold microcombination glass electrode and a Fisher pH-meter (model 815 MP).

NMR experiments were performed at 30 °C with a 11.75 Tesla (499.496 MHz for $^1H$) Varian Unity*plus* spectrometer. Two-dimensional $^1H$-$^{15}N$ HSQC experiments (Kay et al., 1989) were performed with spectral widths of 6,000 and 3,500 Hz for the $^1H$ and $^{15}N$ dimension, respectively. A typical data matrix consisted of 4,096 × 256 complex data points in the f1($^1H$) × f2($^{15}N$) dimensions, respectively. The water peak was assigned a value of 4.71 ppm and thus used as an internal reference. The $^{15}N$ chemical shift reference was $CH_3NO_2$, which was assigned a value of 380.23 ppm (Live et al., 1984).

Two-dimensional sensitivity-enhanced pulse sequences (Cavanagh et al., 1991; Palmer et al., 1991; Skelton et al., 1993) were employed for the inversion-recovery (Vold et al., 1968), CPMG spin–echo (Meiboom & Gill, 1958), and steady-state NOE (Noggle & Shirmer, 1971) experiments to measure the spin–lattice relaxation rate constants ($R_1$), spin–spin relaxation rate constants ($R_2$), and {$^1H$}-$^{15}N$ steady-state NOEs, respectively, of backbone and arginine side chain $^{15}NH$ groups in rCMTI-III and rCMTI-III*. One-hundred twenty-eight increments of 4K data points each were collected with 16 transients per increment for the $R_1$ and $R_2$ measurements, and with 32 transients per increment for the NOE experiments. A total recycling delay of 4 s was used for the NOE experiments. For the $R_1$ determination, eight data sets were collected corresponding to relaxation periods of 0.008, 0.05, 0.12, 0.25, 0.4, 0.7, 1.1, and 2.5 s; similarly, eight data sets were acquired for the $R_2$ measurement with relaxation intervals of 0.015, 0.032, 0.055, 0.13, 0.23, 0.34, 0.52, and 0.87 s. The NOE measurements were performed in duplicate. A line-broadening factor of 6 Hz was applied to the f2 dimension; a shifted Gaussian window function was used in the f1 dimension. The water signal was digitally filtered out before Fourier transformation (Marion et al., 1989).

### *Determination of $^{15}N$ relaxation parameters and computation of model-free parameters*

$R_1$ and $R_2$ were determined by nonlinear least-squares fitting of experimental peak heights to the following equations:

$$I(t) = I_\infty - (I_\infty - I_0)\exp(-R_1 * t) \quad (4)$$

$$I(t) = I_0 \exp(-R_2 * t), \quad (5)$$

where $t$ is the parametrical relaxation delay in each measurement and $I$ is the long-time steady-state resonance intensity. Uncertainties in peak heights were assessed by the RMS baseline noise level. Heteronuclear NOEs were calculated according to the equation:

$$\eta = I_{sat}/I_{unsat}, \quad (6)$$

in which $I_{sat}$ and $I_{unsat}$ are the experimental peak heights measured from spectra recorded with and without proton irradiation during the recycling delay. Uncertainties were calculated by the sum of the RMS of the uncertainties of peak heights about the RMS baseline noise level for $I_{sat}$ and $I_{unsat}$. Model-free parameters (Lipari & Szabo, 1982a, 1982b)—$S^2$, $\tau_e$, and $R_{ex}$—were computed, using the software, Model-Free (version 3.0), kindly provided by Professor Arthur G. Palmer III of Columbia University, New York.

## Supplementary material in Electronic Appendix

Supplementary material includes two figures showing assigned $^1H$-$^{15}N$ HSQC maps of rCMTI-III and rCMTI-III* and four tables containing experimental $R_1$, $R_2$, and NOE data and computed model-free parameters ($S^2$, $\tau_e$, and $R_{ex}$) of rCMTI-III and rCMTI-III*.

## Acknowledgments

This work was supported by grants from the National Institutes of Health (HL-40789 to R.K. and HL-52235 to L.W.) and the American Heart Association, Kansas Affiliate (KS-95-GS-14 to R.K.). R.K. is supported by an NIH Research Career Development Award (HL-03131). The 11.75 Tesla NMR spectrometer at KSU was purchased with an NSF-EPSCoR grant. This is contribution 97-518-J from the Kansas Agriculture Experiment Station.

## References

Ardelt W, Laskowski M Jr. 1991. Effect of single amino acid replacements on the thermodynamics of the reactive site peptide bond hydrolysis in ovomucoid third domain. *J Mol Biol 220*:1041–1053.

Betz SF. 1993. Disulfide bonds and the stability of globular proteins. *Protein Sci 2*:1551–1558.

Betz SF, Marmorino JL, Saunders AJ, Doyle DF, Young GB, Pielak GJ. 1996. Unusual effects of an engineered disulfide on global and local protein stability. *Biochemistry 35*:7422–7428.

Bhaskaran R, Prabhakaran M, Jayaraman G, Yu C, Ponnuswamy PK. 1996. Internal packing conditions and fluctuations of amino acid residues in globular proteins. *J Biomol Struct Dynam 13*:627–639.

Bode W, Epp O, Huber R, Laskowski M Jr, Ardelt W. 1985. The crystal and molecular structure of the third domain of silver pheasant ovomucoid (OMSVP3). *Eur J Biochem 147*:387–395.

Bode W, Greyling HJ, Huber R, Otlewski J, Wilusz T. 1989. The refined 2.0 Å X-ray crystal structure of the complex formed between bovine beta trypsin and CMTI-I, a trypsin inhibitor from squash seeds (*Cucurbita maxima*) Topological similarity of the squash seed inhibitors with the carboxypeptidase A inhibitor from potatoes. *FEBS Lett 242*:285–292.

Bode W, Huber R. 1992. Natural protein proteinase inhibitors and their interaction with proteinases. *Eur J Biochem 204*:433–451.

Buck M, Boyd J, Redfield C, MacKenzie DA, Jeenes DJ, Archer DB, Dobson CM. 1995. Structural determinants of protein dynamics: Analysis of $^{15}N$ NMR relaxation measurements for main-chain and side-chain nuclei of hen egg white lysozyme. *Biochemistry 34*:4041–4055.

Cai M, Gong Y, Kao JLF, Krishnamoorthi R. 1995a. Three-dimensional solution structure of *Cucurbita maxima* trypsin inhibitor-V determined by NMR spectroscopy. *Biochemistry 34*:5201–5211.

Cai M, Gong Y, Prakash O, Krishnamoorthi R. 1995b. Reactive-site hydrolyzed *Cucurbita maxima* trypsin inhibitor-V: Function, thermodynamic stability, and NMR solution structure. *Biochemistry 34*:12087–12094.

Cai M, Huang Y, Prakash O, Wen L, Dunkelbarger SP, Huang JK, Liu J, Krishnamoorthi R. 1996. Differential modulation of binding loop flexibility and stability by $Arg^{50}$ and $Arg^{52}$ in *Cucurbita maxima* trypsin inhibitor-V deduced by trypsin-catalyzed hydrolysis and NMR spectroscopy. *Biochemistry 35*:4784–4794.

Cavanagh J, Palmer AG III, Wright PE, Rance M. 1991. Sensitivity improvement in proton-detected two-dimensional heteronuclear relay spectroscopy. *J Magn Reson 91*:429–436.

Daragan VA, Mayo KH. 1996. Analysis of internally restricted correlated rotations in peptides and proteins using $^{13}C$ and $^{15}N$ NMR relaxation data. *J Phys Chem 100*:8378–8388.

Fersht AR. 1985. *Enzyme structure and mechanism, 2nd ed.* New York: Freeman. pp 405–413.

Fitter J, Lechner RE, Büldt G, Dencher NA. 1996. Internal molecular motions of bacteriorhodopsin: Hydration-induced flexibility studied by quasielastic incoherent neutron scattering using oriented purple membranes. *Proc Natl Acad Sci USA 93*:7600–7605.

Fujinaga M, Read RJ, Sielecki A, Ardelt W, Laskowski M Jr, James MNG. 1982. Refined crystal structure of the molecular complex of *Streptomyces griseus* protease B, a serine protease, with the third domain of the ovomucoid inhibitor from turkey. *Proc Natl Acad Sci USA 79*:4868–4872.

Hayashi K, Takehisa T, Hamato N, Takano R, Hara S, Miyata T, Kato H. 1994. Inhibition of serine proteases of the blood coagulation system by squash family protease inhibitors. *J Biochem Tokyo 116*:1013–1018.

Hinck AP, Truckses DM, Markley JL. 1996. Engineered disulfide bonds in staphylococcal nuclease: Effects on the stability and conformation of the folded protein. *Biochemistry 35*:10328–10338.

Hojima Y, Pierce JV, Pisano JJ. 1982. Pumpkin seed inhibitor of human factor XIIa (activated Hageman factor) and bovine trypsin. *Biochemistry 21*:3741–3746.

Holak TA, Bode W, Huber R, Otlewski J, Wilusz T. 1989a. Nuclear magnetic resonance solution and X-ray structures of squash trypsin inhibitor exhibit the same conformation of the proteinase binding loop. *J Mol Biol 210*:649–654.

Holak TA, Gondol D, Otlewski J, Wilusz T. 1989b. Determination of the complete three-dimensional structure of the trypsin inhibitor from squash seeds in aqueous solution by nuclear magnetic resonance and a combination of distance geometry and dynamical simulated annealing. *J Mol Biol 210*:635–648.

Holak TA, Habazettl J, Oschkinat H, Otlewski J. 1991. Structures of proteins in solution derived from homonuclear three-dimensional NOE–NOE nuclear magnetic resonance spectroscopy. High-resolution structure of squash trypsin inhibitor. *J Am Chem Soc 113*:3196–3198.

Karplus M. 1986. Internal dynamics of proteins. *Methods Enzymol 131*:283–307.

Karplus M, McCammon JA. 1983. Dynamics of proteins: Elements and function. *Annu Rev Biochem 52*:263–300.

Kay LE, Muhandiram DR, Farrow NA, Aubin Y, Forman-Kay JD. 1996. Correlation between dynamics and high affinity binding in an SH2 domain interaction. *Biochemistry 35*:361–368.

Kay LE, Torchia DA, Bax A. 1989. Backbone dynamics of proteins as studied by $^{15}N$ inverse detected heteronuclear NMR spectroscopy: Application to staphylococcal nuclease. *Biochemistry 28*:8972–8979.

Kojima S, Kumagai I, Miura K. 1993. Requirement for a disulfide bridge near the reactive-site of protease inhibitor SSI (*Streptomyces* Subtilisin Inhibitor) for its inhibitory action. *J Mol Biol 230*:395–399.

Krezel AM, Darba P, Robertson AD, Fejzo J, Macura S, Markley JL. 1994. Solution structure of turkey ovomucoid third domain as determined from nuclear magnetic resonance data. *J Mol Biol 242*:203–214.

Krishnamoorthi R, Gong Y, Richardson M. 1990. A new protein inhibitor of trypsin and activated Hageman factor from pumpkin (*Cucurbita maxima*) seeds. *FEBS Lett 273*:163–167.

Krishnamoorthi R, Gong Y, Sun Lin CL, VanderVelde D. 1992a. Two-dimensional NMR studies of squash family inhibitors. Sequence-specific proton assignments and secondary structure of reactive-site hydrolyzed *Cucurbita maxima* trypsin inhibitor III. *Biochemistry 31*:898–904.

Krishnamoorthi R, Lin CLS, VanderVelde D. 1992b. Structural consequences of the natural substitution, E9K, on reactive-site-hydrolyzed squash (*Cucurbita maxima*) trypsin inhibitor (CMTI), as studied by two-dimensional NMR. *Biochemistry 31*:4965–4969.

Krishnamoorthi R, Nemmers S, Tobias B. 1992c. Natural abundance $^{15}N$ NMR assignments delineate structural differences between intact and reactive-site hydrolyzed *Cucurbita maxima* trypsin inhibitor III. *FEBS Lett 304*:149–152.

Laemmli UK. 1970. Cleavage of structural proteins during the assembly of the head of bacteriophage T4. *Nature 227*:680–685.

Laskowski M Jr, Kato I. 1980. Protein inhibitors of proteinases. *Ann Rev Biochem 49*:593–626.

Lehle K, Kohnert U, Stern A, Popp F, Jaenicke R. 1996. Effect of disulfide bonds on the structure, function, and stability of the trypsin/tPA inhibitor from *Erythrina caffra*: Site-directed mutagenesis, expression, and physiochemical characterization. *Nature Biotech 14*:476–480.

Lipari G, Szabo A. 1982a. Model-free approach to the interpretation of nuclear magnetic resonance relaxation in macromolecules. 1. Theory and range of validity. *J Am Chem Soc 104*:4546–4559.

Lipari G, Szabo A. 1982b. Model-free approach to the interpretation of nuclear magnetic resonance relaxation in macromolecules. 2. Analysis of experimental results. *J Am Chem Soc 104*:4559–4570.

Liu J, Prakash O, Cai M, Gong Y, Huang Y, Wen L, Wen JJ, Huang JK, Krishnamoorthi R. 1996a. Solution structure and backbone dynamics of recombinant *Cucurbita maxima* trypsin inhibitor-V determined by NMR spectroscopy. *Biochemistry 35*:1516–1524.

Liu J, Prakash O, Huang Y, Wen L, Wen JJ, Huang JK, Krishnamoorthi R. 1996b. Internal mobility of reactive-site-hydrolyzed recombinant *Cucurbita maxima* trypsin inhibitor-V characterized by NMR spectroscopy: Evidence for differential stabilization of newly formed C- and N-termini. *Biochemistry 35*:12503–12510.

Live DH, Davis DG, Agosta WC, Cowburn D. 1984. Observation of 1000-fold enhancement of nitrogen-15 NMR via proton-detected multiquantum coherences: Studies of large peptides. *J Am Chem Soc 106*:6104–6105.

Marion D, Ikura M, Bax A. 1989. Improved solvent suppression in one- and two-dimensional NMR spectra by convolution of time-domain data. *J Magn Reson 84*:425–430.

Mchaourab HS, Oh KJ, Fang CJ, Hubbell WL. 1997. Conformation of T4 lysozyme in solution. Hinge-bending motion and the substrate-induced conformational transition studied by site-directed spin labeling. *Biochemistry 36*:307–316.

McWherter CA, Walkenhorst WF, Campbell EJ, Glover GI. 1989. Novel inhibitors of human leukocyte elastase and cathepsin G. Sequence variants of squash seed protease inhibitor with altered protease selectivity. *Biochemistry 28*:5708–5714.

Meiboom S, Gill D. 1958. Modified spin-echo method for measuring nuclear relaxation times. *Rev Sci Instr 29*:688–691.

Musil D, Bode W, Huber R, Laskowski M Jr, Lin TY, Ardelt W. 1991. Refined X-ray crystal structures of the reactive site modified ovomucoid inhibitor third domains from silver pheasant (OMSVP3*) and from Japanese quail (OMJPQ3*). *J Mol Biol 220*:739–755.

Nemmers S. 1992. Structural differences between intact and reactive-site hydrolyzed *Cucurbita maxima* trypsin inhibitor III, as studied by proton-detected natural abundance $^{15}N$ and $^{13}C$ heteronuclear NMR spectroscopy [thesis]. Manhattan, Kansas: Kansas State University.

Nicholson LK, Kay LE, Baldisseri DM, Arango J, Young PE, Bax A, Torchia DA. 1992. Dynamics of methyl groups in proteins as studied by proton-detected $^{13}C$ NMR spectroscopy. Application to the leucine residues of staphylococcal nuclease. *Biochemistry 31*:5253–5263.

Noggle JH, Shirmer RE. 1971. *The nuclear Overhauser effect: Chemical applications.* New York: Academic Press.

Oschkinat H, Muller T, Dieckmann T. 1994. Protein structure determination with three- and four-dimensional NMR spectroscopy. *Angew Chem Int Ed 33*:277–293.

Otlewski J, Krowarsch D. 1996. Squash inhibitor family of serine proteinases. *Acta Biochim Pol 43*:431–444.

Otlewski J, Zbyryt T. 1994. Single peptide bond hydrolysis/resynthesis in squash inhibitors of serine proteinases. 1. Kinetics and thermodynamics of the interaction between squash inhibitors and bovine $\beta$-trypsin. *Biochemistry 33*:200–207.

Otlewski J, Zbyryt T, Krokoszynska I, Wilusz T. 1990. Inhibition of serine proteinases by squash inhibitors. *Biol Chem Hoppe Seyler 371*:589–594.

Palmer AG III, Rance M, Wright PE. 1991. Intramolecular motions of a zinc finger DNA-binding domain from Xfin characterized by proton-detected natural abundance carbon-13 heteronuclear NMR spectroscopy. *J Am Chem Soc 113*:4371–4380.

Papamokos E, Weber E, Bode W, Huber R, Empie MW, Kato I, Laskowski M Jr. 1982. Crystallographic refinement of japanese quail ovomucoid, a Kazal-type inhibitor, and model building studies of complexes with serine proteases. *J Mol Biol 158*:515–537.

Peng JW, Wagner G. 1994. Investigation of protein motions via relaxation measurements. *Methods Enzymol 239*:563–596.

Qasim MA, Ganz PJ, Saunders CW, Bateman KS, James MNG, Laskowski M Jr. 1997. Interscaffolding additivity. Association of $P_1$ variants of eglin *c* and of turkey ovomucoid third domain with serine proteinases. *Biochemistry 36*:1598–1607.

Richards FM. 1992. Folded and unfolded proteins: An introduction. In: Creighton TE, ed. *Protein folding*. New York: Freeman. pp 1–58.

Rosenfeld R, Vajda S, Delisi C. 1995. Flexible docking and design. *Annu Rev Biophys Biomol Struct 24*:677–700.

Sambrook J, Fritsch EF, Maniatis T. 1989. *Molecular cloning: A laboratory manual, 2nd ed.* Cold Spring Harbor, New York: Cold Spring Harbor Laboratory Press.

Schechter I, Berger M. 1967. On the size of the active site in proteases. I. Papain. *Biochem Biophys Res Commun 27*:157–162.

Skelton NJ, Palmer AG III, Akke M, Kördel J, Rance M, Chazin WJ. 1993. Practical aspects of two-dimensional proton-detected $^{15}N$ spin relaxation measurements. *J Magn Reson Ser B 102*:253–264.

Vajda S, Weng ZP, Rosenfeld R, Delisi C. 1994. Effect of conformational flexibility and solvation on receptor–ligand binding free energies. *Biochemistry 33*:13977–13988.

Vold RL, Waugh JS, Klein MP, Phelps DE. 1968. Measurement of spin relaxation in complex systems. *J Chem Phys 48*:3831–3832.

Walkenhorst WF, Krezel AM, Rhyu GI, Markley JL. 1994. Solution structure of reactive-site hydrolyzed turkey ovomucoid third domain by nuclear magnetic resonance and distance geometry methods. *J Mol Biol 242*:215–230.

Weber E, Papamokos E, Bode W, Huber R, Kato I, Laskowski M Jr. 1981. Crystallization, crystal structure analysis and molecular model of the third domain of Japanese quail ovomucoid, a Kazal type inhibitor. *J Mol Biol 149*:109–123.

Wen L, Kim SS, Tinn TT, Huang JK, Krishnamoorthi R, Gong Y, Lwin YN, Kyin S. 1993. Chemical synthesis, molecular cloning, overexpression, and site-directed mutagenesis of the gene coding for pumpkin (*Curcubita maxima*) trypsin inhibitor, CMTI-V. *Protein Express Purif 4*:215–222.

Wen L, Lee I, Chen GJ, Huang JK, Gong Y, Krishnamoorthi R. 1995. Changing the inhibitory specificity and function of *Cucurbita maxima* trypsin inhibitor-V by site-directed mutagenesis. *Biochem Biophys Res Commun 207*:897–902.

Wieczorek M, Otlewski J, Cook J, Parks K, Leluk J, Wilimowska-pelc A, Polanowski A, Wilusz T, Laskowski M Jr. 1985. The squash family of serine proteinase inhibitors: Amino acid sequences and association equilibrium constants of inhibitors from squash *Cucurbita maxima*, summer squash, zucchini, *Cucurbita pepo* cultivar giromontia and cucumber *Cucumis sativus* seeds. *Biochem Biophys Res Commun 126*:646–652.

Wynn R, Laskowski M Jr. 1990. Inhibition of human $\beta$-factor $XII_A$ by squash family serine proteinase inhibitors. *Biochem Biophys Res Commun 166*:1406–1410.